Structural and Kinetic Study of Differences between Human and Escherichia coli Manganese Superoxide Dismutases †

5 AUTHORS, INCLUDING:

John Domsic
University of Pennsylvania
21 PUBLICATIONS   349 CITATIONS

SEE PROFILE

Diane E Cabelli
Brookhaven National Laboratory
91 PUBLICATIONS   3,150 CITATIONS

SEE PROFILE

Robert Mckenna
University of Florida
239 PUBLICATIONS   5,095 CITATIONS

SEE PROFILE

Structural and Kinetic Study of Differences between Human and *Escherichia coli* Manganese Superoxide Dismutases[†]

Jiayin Zheng,[‡] John F. Domsic,[§] Diane Cabelli,[||] Robert McKenna,*,[§] and David N. Silverman*,[‡,§]

Department of Pharmacology and Therapeutics and Department of Biochemistry and Molecular Biology, University of Florida, Gainesville, Florida 32610, and Department of Chemistry, Brookhaven National Laboratory, Upton, New York 11973

ABSTRACT: Human manganese superoxide dismutase (MnSOD) is characterized by a product inhibition stronger than that observed in bacterial forms of MnSOD. Previous studies show that the conserved, active-site residue Tyr34 mediates product inhibition; however, the protein environment of Tyr34 is different in human and *Escherichia coli* MnSOD. We have prepared two site-specific mutants of human MnSOD with replacements of Phe66 with Ala and Leu (F66A and F66L, respectively), altering the surroundings of Tyr34. Pulse radiolysis was used to generate superoxide, and measurements of catalysis were taken in single-turnover experiments by observing the visible absorbance of species of MnSOD and under catalytic conditions observing the absorbance of superoxide. The mutation of Phe66 to Leu resulted in a mutant of human MnSOD with weakened product inhibition resembling that of *E. coli* MnSOD. Moreover, the mechanism of this weakened product inhibition was similar to that in *E. coli* MnSOD, specifically a decrease in the rate constant for the oxidative addition of superoxide to Mn^{2+}MnSOD leading to the formation of the peroxide-inhibited enzyme. In addition, the crystal structures of both mutants have been determined and compared to those of wild-type human and *E. coli* MnSOD. The crystallographic data suggest that the solvent structure and its mobility as well as side chain conformations may affect the extent of product inhibition. These data emphasize the role of residue 66 in catalysis and inhibition and provide a structural explanation for differences in catalytic properties between human and certain bacterial forms of MnSOD.

Manganese superoxide dismutase (MnSOD)[1] confers defense against the toxic effects of reactive oxygen species by catalyzing the dismutation of the superoxide radical anion ($O_2^{•−}$) into O_2 and H_2O_2 (*1−3*). Human MnSOD is a mitochondrial enzyme, a homotetramer of 22 kDa subunits constructed as a dimer of dimers with dimeric and tetrameric interfaces (*4*). Although the active-site residues of human

and *Escherichia coli* MnSOD are superimposable in the vicinity of the manganese ion (Figure 1), MnSOD from *E. coli* as well as from many prokaryotes is a dimer. The active site of MnSOD contains one manganese ion which is coordinated in a trigonal bipyramidal geometry by three histidines, one aspartate, and a bound solvent molecule (Figure 1). Extending from this site is a hydrogen-bonded network involving the side chains of Gln143, Tyr34, and His30 that is highly conserved both in MnSOD and in the very structurally similar FeSOD (*3−6*).

Catalysis of the disproportionation of superoxide by MnSOD proceeds at near-diffusion-controlled rates, during which the manganese ion cycles between Mn^{2+} and Mn^{3+} oxidation states (*2*, *3*). During catalysis by many forms of MnSOD, measured by pulse radiolysis and stopped-flow spectrophotometry, an initial catalytic burst is followed by a region of zero-order decay of superoxide that is best explained by the formation of a product-inhibited complex of MnSOD (*7−9*). The structure of the inhibited complex is not known; however, there is some evidence that it is a side-on peroxo complex of the manganese (*7*). An enhanced zero-order phase corresponds to greater product inhibition, and its magnitude varies among MnSODs from different sources, appearing more prominent in human MnSOD compared with MnSOD from bacterial sources (*7−10*). Previous efforts have attempted to reduce the contribution of the zero-order phase by site-directed mutagenesis of human MnSOD (*11*). The motivation for this effort was the observation that a site-
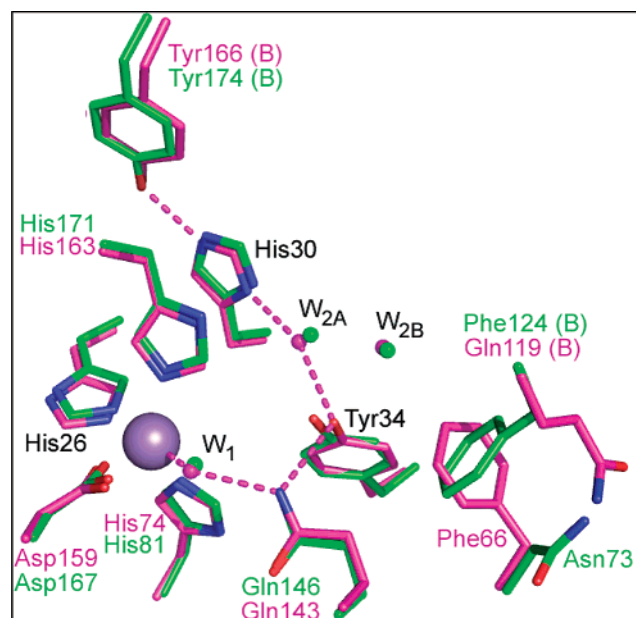
FIGURE 1: Superposition of the active-site cavities of wild-type human MnSOD (magenta) and *E. coli* MnSOD (green). The magenta dashed lines are inferred hydrogen bonds for human wild-type MnSOD. Gln119B in the human and Phe124B in the *E. coli* enzymes are from the adjacent B subunit at the dimeric interface. The structure of human wild-type MnSOD is from Protein Data Bank (PDB) entry 1LUV (*23*) and *E. coli* MnSOD from PDB entry 1D5N (*32*). This figure was made using PYMOL (www.pymol.org).

specific mutant of human MnSOD (H30N MnSOD) with weakened product inhibition is antiproliferative when over-expressed in human cancer cells (*12*). However, efforts to reduce the contribution of zero-order kinetics in human MnSOD through site-specific mutagenesis of active-site residues has resulted mostly in a decreased level of catalysis rather than in maintaining catalysis and weakening product inhibition (*11, 13, 14*).

Here we take advantage of the known structures of human and *E. coli* MnSOD to improve our understanding of the source of the different levels of catalysis and product inhibition between them. There is a large body of data on the role of Tyr34 in catalysis by MnSOD (*15−18*), including evidence that replacing Tyr34 with Phe in human MnSOD produced a significant increase in the rate of product inhibition (*17*). This suggests that the active-site environment in the vicinity of Tyr34 may contribute to product inhibition. The side chains of Tyr34 in human and in *E. coli* MnSOD are in different environments (Figure 1). It was our hypothesis that the residues adjacent to Tyr34 affect the extent of product inhibition and perhaps also catalytic activity, and that these residues may be significant in explaining the different extents of product inhibition in human and *E. coli* MnSOD. We have replaced Phe66 with Ala and Leu at the dimeric interface of human MnSOD to study the effect of the environment of Tyr34 on catalysis and inhibition. Pulse radiolysis was used to generate superoxide to evaluate catalytic and inhibitory properties of these mutants, and their structures were determined using X-ray crystallography. The rate constants for catalysis and product inhibition of a conservative F66L human MnSOD mutant resemble those of the *E. coli* MnSOD and locate a region of MnSOD that mediates product inhibition.

METHODS

Site-Directed Mutagenesis. The mutants were generated with the Stratagene (La Jolla, CA) QuikChange site-directed mutagenesis kit in a Perkin-Elmer (Foster City, CA) Gene-Amp PCR system 2400. The plasmid of wild-type MnSOD contained in the pTrc99A vector was used as the template. PCR was performed using specific oligonucleotides (Sigma-Genosys, The Woodlands, TX) containing the desired mutations (underlined) as primers (designated primers 1 and 2). The following primers were used: F66A primer 1 (5′ CCTGCACTGAAGGCCAATGGTGGTGG 3′) and F66A primer 2 (5′ CCACCACCATTGGCCTTCAGTGCAGG 3′) and F66L primer 1 (5′ GCCTGCACTGAAG-CTCAATG-GTGGTGGTC 3′) and F66L primer 2 (5′ GACCACCAC-CATTGAGCTTCAG-TGCAGGC 3′). The PCR products were digested with the restriction enzyme *Dpn*I and trans-formed into supercompetent XL-1 cells for selection. The plasmid containing the mutation of interest was isolated using the plasmid miniprep kit from Qiagen, and the mutation was corroborated by DNA sequencing of the entire coding region (ICBR, University of Florida). The plasmid containing the desired mutation was then transformed into QC774 cells from *E. coli*. This particular strain lacks the genes that encode endogeneous FeSOD (*SodB⁻*) and MnSOD (*SodA⁻*) (*19*).

Enzyme Expression and Purification. *E. coli* cells that expressed the site-directed mutants of human MnSOD were grown for 16 h at 37 °C in 50 mL of LB medium. The overnight culture was transferred to 6.0 L of 2×YT medium supplemented with 100 μg/mL ampicillin and 10 mM MnCl$_2$. The cells were allowed to grow for ~4 h until an OD$_{600}$ of 0.5 was reached. At this point, the cells were induced with 0.3 mM IPTG and were allowed to grow for an additional 4 h. The cells were then placed at 4 °C overnight and harvested the next day by centrifugation. The resulting pellet was frozen at −70 °C until lysis was performed.

The pellet was resuspended in lysis buffer [32 mM Tris-HCl (pH 8.2), 2.7 M glycerol, 0.2 mM EDTA, 0.2% Triton X-100, 0.4 mg/mL lysozyme, and 0.02 mg/mL DNase I] and stirred for 3 h. The suspension of lysed cells was spun down, and the supernatant was heated at 60 °C for 10 min and then spun down to remove the precipitate. The resulting super-natant was dialyzed overnight against 4 L of 10 mM Tris-HCl (pH 8.2) containing 0.1 mM EDTA. After the third dialysis step, the solution was filtered, and anion exchange chromatography was performed to further separate MnSOD from some cellular proteins still present after the heating and extensive dialysis. The purified protein was concentrated (15 mg/mL) in a final buffer of 20 mM potassium phosphate (pH 7.8). The purity was determined by SDS−polyacryla-mide gel electrophoresis, where one intense band at 22 kDa indicated the presence of the monomer form of MnSOD. Nondenaturing polyacrylamide gel electrophoresis on human wild-type, F66A, and F66L MnSOD showed that all migrated at an equal rate consistent with a tetrameric structure. MnSOD from *E. coli* is dimeric and from human MnSOD is tetrameric (*1, 4, 20*). The amount of manganese present was determined using ICP-MS (inductively coupled plasma mass spectrometry). Concentrations of the active enzyme were taken as the manganese concentration.

Pulse Radiolysis. All pulse radiolysis experiments were performed at Brookhaven National Laboratory, using the 2

MeV van de Graaff accelerator as described by Cabelli et al. (*21*). Solutions at 25 °C contained enzyme, 30 mM sodium formate, 50 μM EDTA, and one of the following buffers (at 2 mM) depending upon the pH of the experiment: HEPES at pH 6.4−7.9, TAPS at pH 8.0−8.8, or CHES at pH 8.9−10.9.

Crystallization. The enzyme samples were crystallized using the hanging drop vapor diffusion method. The drops consisted of 5 μL of enzyme mixed with 5 μL of precipitant solution [2.5 M ammonium sulfate, 100 mM imidazole, and 100 mM malic acid (pH 8.5)] and suspended over 1 mL of precipitant solution. The crystals grew at room temperature (RT) to full size in approximately 1 week.

Data Collection and Refinement. X-ray diffraction data were collected using a Rigaku HU-H3R CU rotating anode generator, Osmic mirrors, a 0.3 mm collimator, and an R-AXIS IV^{++} image plate system. Data were collected at RT with a crystal-to-detector distance of 190 mm. We have not been able to find a suitable cryoprotectant for which the mosaic spread of the lattice is sufficiently sustained to permit collection of data that are equal to our current data at room temperature. A total of 45° of data was collected with 0.25° oscillations and an exposure time of 5 min from a single crystal of the F66L MnSOD mutant, and a total of 90° of data was collected (45° each) from two F66A MnSOD mutant crystals. X-ray data processing was performed using DENZO, and data were scaled and reduced with SCALEPACK (*22*).

Initial direct attempts at phasing, using the previously reported isomorphous crystal structure of wild-type human MnSOD [Protein Data Bank (PDB) entry 1LUV (*23*)] with all solvent molecules removed, were unsuccessful. Therefore, phases were determined via standard molecular replacement methods using *Molrep* from the CCP4 suite of software (*24, 25*) with the coordinates of wild-type human MnSOD. This showed that one of the crystallographic 2-fold axes coincided with the tetrameric interfacial 2-fold axis of the human MnSOD tetramer. Usually, for hexagonal space group *P*6₁-22, this overlap occurs at the dimeric interfacial 2-fold axis, and therefore, this was the reason why the initial direct phasing had been unsuccessful.

To avoid any potential phase bias and to accurately determine the position of the side chains, residues Tyr34, Phe66, and Gln119 were also mutated to alanines. Both structures were further refined using the Crystallography and NMR Systems (CNS) suite of programs (*26*). Refinement included an initial round of simulated annealing followed by energy minimization and *B*-factor assignment, after which residues Tyr34, Phe66, and Gln119 were reintroduced into the structures. The structures were then further refined, and water picking was performed. The $2F_o − F_c$ and $F_o − F_c$ Fourier electron density maps were then generated, and the atomic positions were further modeled using *Coot* (*27*). The human F66A MnSOD structure was refined to 2.2 Å resolution with a final R_{factor} of 19.5%. Similarly, human F66L MnSOD was refined to 2.3 Å resolution with a final R_{factor} of 19.9%. The X-ray data collection and final model refinement statistics for both structures are given in Table 1. Because of the large *c*-axis unit cell vector for both mutants F66A and F66L (∼242 Å), we were unable to collect higher-resolution Bragg reflections in certain crystal orientations. Due to the inherent problem of reflection overlap,

Table 1: Data and Refinement Statistics for Human F66A and F66L MnSOD Crystal Structures[a]

	F66A	F66L
resolution (Å)	20−2.2 (2.28−2.20)	20−2.3 (2.38−2.30)
R_{sym}[b] (%)	8.0 (17.0)	7.3 (13.1)
completeness (%)	93.7 (88.0)	92.6 (90.4)
redundancy	5.2 (3.7)	3.1 (2.8)
unit cell (Å)	$a = 81.16$, $c = 242.77$	$a = 81.08$, $c = 242.52$
space group	$P6_122$	$P6_122$
$I/I(\sigma)$	31.2	38.4
R_{factor}[c] (%)	19.5	19.9
R_{free}[d] (%)	21.7	20.55
no. of atoms (main/solvent)	1560/68	1552/71
average *B*-factor (Å²) (main/side/solvent)	24.5/27.7/33.1	22.8/25.5/24.1
rmsd for distances (Å)	0.008	0.007
rmsd for angles (deg)	1.4	1.3

[a] Data in parentheses are for the highest-resolution shell. [b] $R_{sym} = (\sum|I − \langle I \rangle|/\sum\langle I \rangle) \times 100$. [c] $R_{factor} = (\sum|F_o| − |F_c|/\sum|F_{obs}|) \times 100$. [d] R_{free} is calculated like R_{work}, except it uses 5% of reflection data omitted from refinement.
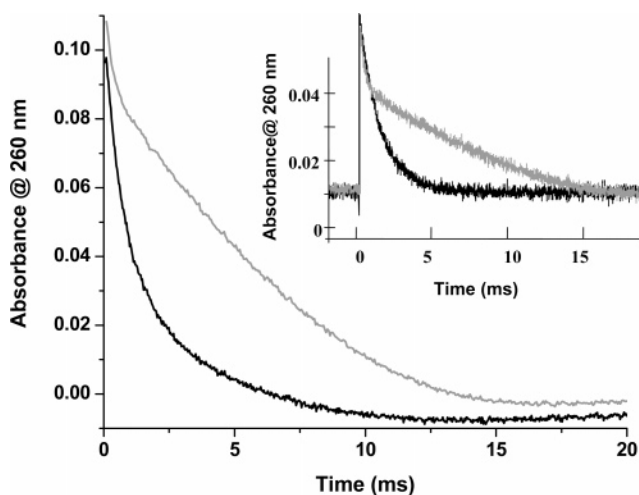

FIGURE 2: Decrease in the absorbance at 260 nm during catalysis by human F66A MnSOD (gray) and F66L MnSOD (black). The initial concentration of $O_2^{•−}$ was 30 μM, generated by pulse radiolysis. The F66A and F66L MnSOD concentrations were 2.4 and 2.9 μM, respectively. Solutions also contained 30 mM formate, 50 μM EDTA, and 2 mM CHES at pH 8.6 and 25 °C. The inset shows the decrease in absorbance at 260 nm measuring superoxide disappearance during catalysis by human MnSOD (gray) and *E. coli* MnSOD (black). The initial superoxide concentration was 10 μM and that of MnSOD 1 μM.

intensity measurements were less reliable and higher-resolution shell measurements less than complete. The atomic coordinates for the human F66A and F66L MnSOD structures have been deposited in the PDB as entries 2QKA and 2QKC, respectively.

RESULTS

Catalysis. Catalysis of the dismutation of superoxide was assessed from the rate of decrease of absorbance of superoxide at 260 nm [$\epsilon_{260} = 2000$ M$^{−1}$ cm$^{−1}$ (*28*)] using pulse radiolysis to generate superoxide. Under similar conditions of initial superoxide and enzyme concentrations, the decay of superoxide catalyzed by human F66L MnSOD was more rapid than that for human F66A (Figure 2). Catalysis by F66A MnSOD showed an initial burst of activity followed by a region of predominantly zero-order rate representing

product inhibition (*7, 8*), a property displayed by human wild-type MnSOD (*9*). The data in Figure 2 for F66A MnSOD were fit to a sum of a first-order process in $O_2^{\bullet-}$ (unsaturated catalytic) and a zero-order process (product inhibited) with a zero-order rate constant $k_0/[E]$ of 1740 s^{-1} (the second-order decrease in $O_2^{\bullet-}$ representing uncatalyzed decay of $O_2^{\bullet-}$ was a minor contribution and subtracted). F66A MnSOD was almost 3 times less inhibited than wild-type MnSOD which has a $k_0/[E]$ value of 500 s^{-1} (*11*). The mutant F66L MnSOD appeared to be uninhibited as determined from the lack of a zero-order region and was much more efficient at removing $O_2^{\bullet-}$ (Figure 2). In these catalyses, F66L MnSOD resembled MnSOD from *E. coli* in that no product inhibition was apparent (Figure 2, inset).

The simplified kinetic scheme of eqs 1–4 has been used in many studies to describe catalysis by MnSOD (*8, 11*). In this scheme, eqs 1 and 2 represent the uninhibited oxidation–reduction cycle by which MnSOD catalyzes the dismutation. The scheme is written here to reflect the observation that MnSOD takes up a proton upon reduction of the metal, shown as $Mn^{2+}SOD(H^+)$ in eqs 1 and 2; in addition, the protonated site is suggested to be a solvent ligand of the metal (*29*). Equations 3 and 4 represent the formation and dissociation, respectively, of the product-inhibited complex in which $Mn^{3+}(O_2^{2-})SOD(H^+)$ represents the inhibited complex.

$$Mn^{3+}SOD + O_2^{\bullet-} \xrightarrow{k_1(+H^+)} Mn^{2+}SOD(H^+) + O_2 \qquad (1)$$

$$Mn^{2+}SOD(H^+) + O_2^{\bullet-} \xrightarrow{k_2(+H^+)} Mn^{3+}SOD + H_2O_2 \qquad (2)$$

$$Mn^{2+}SOD(H^+) + O_2^{\bullet-} \xrightarrow{k_3} Mn^{3+}(O_2^{2-})SOD(H^+) \qquad (3)$$

$$Mn^{3+}(O_2^{2-})SOD(H^+) \xrightarrow{k_4(+H^+)} Mn^{3+}SOD + H_2O_2 \qquad (4)$$
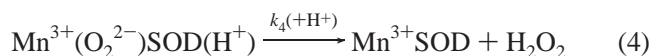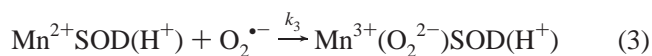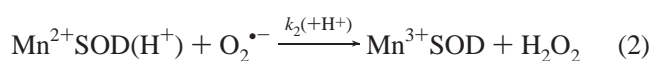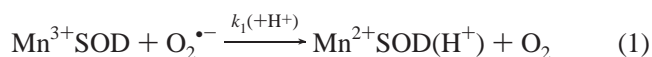
Values of the rate constants k_1–k_4 were measured by following the change in absorbance of superoxide and of enzyme species in single-turnover experiments following the generation of superoxide by pulse radiolysis (*11, 21*). For example, introducing $O_2^{\bullet-}$ into a sample of oxidized enzyme allowed us to measure the rate constant k_1 by following the decrease in absorbance at 480 nm of $Mn^{3+}SOD$ [$\epsilon_{480} = 610$ M^{-1} cm^{-1} (*30*)]. Pretreating the enzyme with a slight molar excess of H_2O_2 efficiently reduced the enzyme to $Mn^{2+}SOD$ ($\epsilon_{480} < 30$ M^{-1} cm^{-1}). Then after pulse radiolysis, reaction of $O_2^{\bullet-}$ resulted in the appearance of oxidized enzyme determined from the 480 nm peak from which k_2 was measured; a typical result is given in Figure 3. The rate constant k_3 was estimated from the appearance of a peak at 420 nm characteristic of the product-inhibited form ($\epsilon_{420} = 500$ M^{-1} cm^{-1}), and k_4 was determined by observing the increase at 480 nm and the concurrent decrease at 420 nm corresponding to decay of the product-inhibited complex. Because of a smaller extent of formation of the product-inhibited complex, another procedure was used for human F66L MnSOD as with *E. coli* MnSOD in which k_2–k_4 were determined from the catalyzed decay of superoxide such as that shown in Figure 2 using the Numerical Integration of Chemical Kinetics program in PRWIN (H. Schwartz, Brookhaven National Laboratory).
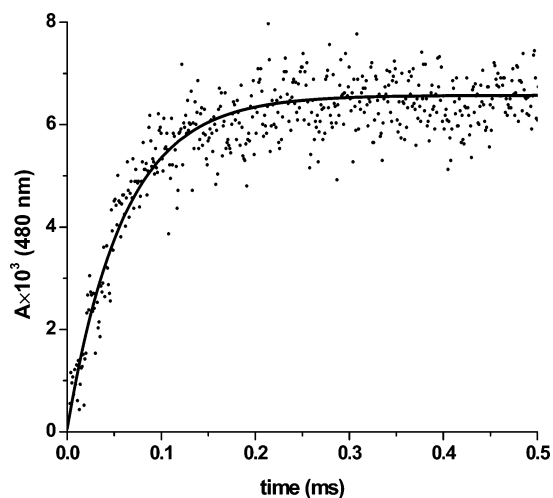

FIGURE 3: Increase in absorbance at 480 nm of 45 μM human F66L MnSOD at times after pulse radiolysis which generated an initial superoxide concentration of 5 μM. Solutions contained 30 mM formate, 50 μM EDTA, and 2 mM CHES at pH 8.6 and 25 °C. The enzyme had been reduced by the addition of H_2O_2. The solid line is a fit to a first-order process corresponding to a k_2 of 0.40 ± 0.03 nM^{-1} s^{-1}.

Table 2: Values of the Rate Constants k_1–k_4 (eqs 1–4) for Catalysis by Human Wild-Type, F66A, and F66L MnSOD and Wild-Type *E. coli* MnSOD Obtained by Pulse Radiolysis

enzyme	k_1 (nM^{-1} s^{-1})	k_2 (nM^{-1} s^{-1})	k_3 (nM^{-1} s^{-1})	k_4 (s^{-1})
wild-type human[a]	1.5	1.1	1.1	120
F66A[b]	0.6	0.5	0.7	82
F66L[b]	0.7	0.8	0.2	40
wild-type *E. coli*[c]	1.1	0.9	0.2	60

[a] From ref *11*. Data obtained at pH 8.2 and 25 °C. [b] Solutions contained 30 μM enzyme, 30 mM formate, 50 μM EDTA, and 2 mM HEPES at pH 8.0. All data were collected at 25 °C. Experimental uncertainties in rate constants are no greater than 15%. [c] From ref *10*.

The results of the studies using pulse radiolysis are summarized in Table 2 for data at pH 8, near the pH expected for the mitochondrial matrix (*31*). Both mutants F66A and F66L MnSOD showed slight reductions of ~2-fold in the rate constant k_1 compared with that of human wild-type MnSOD. Although the mutants have decreased values of k_2 and k_3 compared with those of the wild type, the value of k_3 for F66L represents the greatest change (Table 2). The rate constants for F66L MnSOD then appear more similar to those observed for *E. coli* MnSOD than to those of the human wild type (Table 2).

As with human wild-type MnSOD, there was no significant pH dependence of k_1–k_3 for F66A and F66L MnSOD over the pH range of 6.5–8.5; these rate constants decreased slightly at pH > 8.5 but could not be fit to a single ionization (data not shown). The pH profile of k_4 for F66L MnSOD, as with human wild-type MnSOD, was independent of pH over the pH range of 7–10. The pH profile of k_4 for F66A MnSOD appeared to increase in a linear manner from 65 s^{-1} at pH 7 to 150 s^{-1} at pH 10, although there was increased experimental error (20%) at pH > 8 (see the Supporting Information).

Further evidence of product inhibition was obtained via examination of the formation of enzyme species after the introduction of superoxide by pulse radiolysis. These experi-
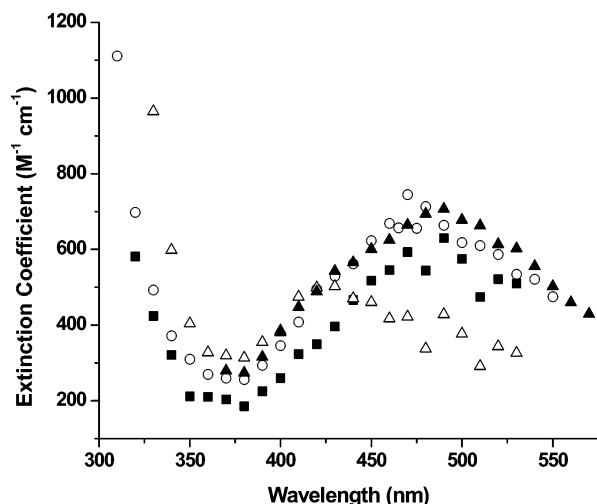
FIGURE 4: Extinction coefficient ϵ (M^{-1} cm^{-1}) as a function of wavelength upon pulse radiolysis of a solution containing wild-type human MnSOD obtained ($\triangle$) short times (0.2–1.0 ms) after introduction of superoxide and showing a maximum at 420 nm characteristic of the intermediate product-inhibited state and ($\blacksquare$) after longer times (>50 ms) showing the enzyme returned to the oxidized state, Mn^{3+}SOD. The same experiment for *E. coli* ($\bigcirc$) and F66L ($\blacktriangle$) MnSOD showed no intermediate at 420 nm. Experimental conditions were as described in the legend of Figure 2.

ments were performed at varying wavelengths across the visible spectrum. Data for human wild-type MnSOD showed the presence of a reversible intermediate state at short times after introduction of $O_2^{\bullet-}$ (measurements began 0.2 ms after introduction of superoxide and extended to 1.0 ms) and were characterized by a maximum near 420 nm which has typified the product-inhibited state (Figure 4). At longer times, the spectrum reverted to that of the oxidized enzyme Mn^{3+}SOD with a maximum at 480 nm (Figure 4). However, examination of these time ranges for F66L and *E. coli* MnSOD showed no evidence of such an intermediate in the progress curves (Figure 4; again measurements began 0.2 ms after introduction of superoxide).[2] The data for F66A MnSOD (not shown) were complex and did not resemble those of either wild-type or F66L MnSOD.

Crystallography. The overall effects of the replacement of Phe66 with Leu and Ala in human MnSOD are shown in Figure 5. Other than these mutated residues, the two amino acid positions that are affected are Gln119 (from the adjacent subunit at the dimeric interface) and Tyr34. In F66L MnSOD, the presence of Leu66 caused a shift in the side chain of Gln119 to a position approximately 1 Å farther from the active-site manganese than in human wild-type MnSOD (Figure 5). This shift presumably avoids a steric clash of the $\delta2$ carbon of Leu66 with the γ and δ carbons of Gln119. However, the distance between residues 66 and 119 in the F66L mutant is not changed compared to those in human wild-type MnSOD. The F66L replacement also had an effect on the conformation of Tyr34. By reducing the bulk of the

side chain at position 66, the F66L mutation caused the side chain of Tyr34 to shift away from the manganese with the hydroxyl of Tyr34 moving by approximately 0.3 Å (Figure 5), although this movement would require a resolution higher than the current resolution of 2.2 Å to be confirmed.

The replacement of Phe66 with Ala in F66A MnSOD resulted in a dramatic change in the orientation of the side chain of Gln119. The $\beta-\gamma$ carbon torsion angle of Gln119 is rotated approximately 90° compared to that of human wild-type MnSOD, causing the side chain of Gln119 in F66A MnSOD to point toward the active-site manganese, thus occupying the void left by the F66A mutation (Figure 5). Like the F66L mutation, the side chain of Tyr34 shifted away from the manganese, albeit by a larger amount, with the hydroxyl moving by ~0.5 Å.

These movements of residues Gln119 and Tyr34 have additional effects on the positions of two waters, W_{2A} and W_{2B}. Water molecule W_{2A} connects the side chains of Tyr34 and His30 via hydrogen bonds, and water molecule W_{2B} intervenes between W_{2A} and bulk solvent (Figures 1 and 5). Generally, the relative locations of these two waters are the same for the four structures studied in Table 2. W_{2A} is positioned between the hydroxyl of Tyr34 and the $\delta1$ nitrogen of His30, and W_{2B} is located between the hydroxyl of Tyr34 and the positions of residues 66 and 119 (73 and 124 in *E. coli* MnSOD, respectively). The distances of the interactions of W_{2A} and W_{2B} with the hydroxyl of Tyr34 (d_{2A} and d_{2B}, respectively, in Figure 6) are similar for human wild-type, F66A, and F66L MnSOD and *E. coli* MnSOD (Table 3). However, the distance between the two waters (d_{2AB}) changed in the structures of the two human mutants, increasing from 2.9 Å in the wild type to 3.8 Å in F66L and to 4.0 Å in F66A. This had the effect of broadening the solvent accessible area enclosed between the dimeric interface and the active site.

To evaluate the mobility of active-site solvent molecules, a comparison of *B*-factors was made between human wild-type, F66A, and F66L MnSOD and *E. coli* MnSOD. It is important to note that the *E. coli* structure was determined at 100 K (*32*), whereas the human structures were determined at room temperature. Due to dissimilarities in the structure resolution limits, a direct comparison of the *B*-factors was not valid. Therefore, the *B*-factors had to be normalized to the average *B*-factor of the structure to which the atoms belonged. To prevent erroneous normalization of the average *B*-factors due to structural variation between human and *E. coli* MnSOD, the average *B*-factors were based only on those main chain atoms of three regions of conserved tertiary structure for a total of 188 atoms (human, 21–34, 120–126, and 157–175; *E. coli*, 21–34, 125–131, and 165–178) which have an overall rmsd of 0.2 Å. Error bars for the *B*-factors were calculated from the refinement of the MnSOD dimer-associated monomers as independent molecules (without the use of a noncrystallographic operator). The independently refined dimer equivalent pairs of atoms were then used to calculate the standard deviations of their average *B*-factor. Then both the average *B*-factor and its associated standard deviations were normalized and plotted (Figure 7).

The analysis of the normalized *B*-factors showed that the manganese, the side chains of Tyr34 and His30, and solvent molecule W_1 had comparatively well-defined positions in

---

[2] It is noted that product inhibition is observed in human F66L MnSOD and in *E. coli* MnSOD at higher superoxide concentrations. The rate constant of the zero-order phase is independent of superoxide concentration, but for these enzymes, it takes a larger ratio of superoxide to enzyme concentrations to force the system into a product-inhibited mode. This is due to larger k_2/k_3 gating ratios for human F66L MnSOD and in *E. coli* MnSOD (Table 2).
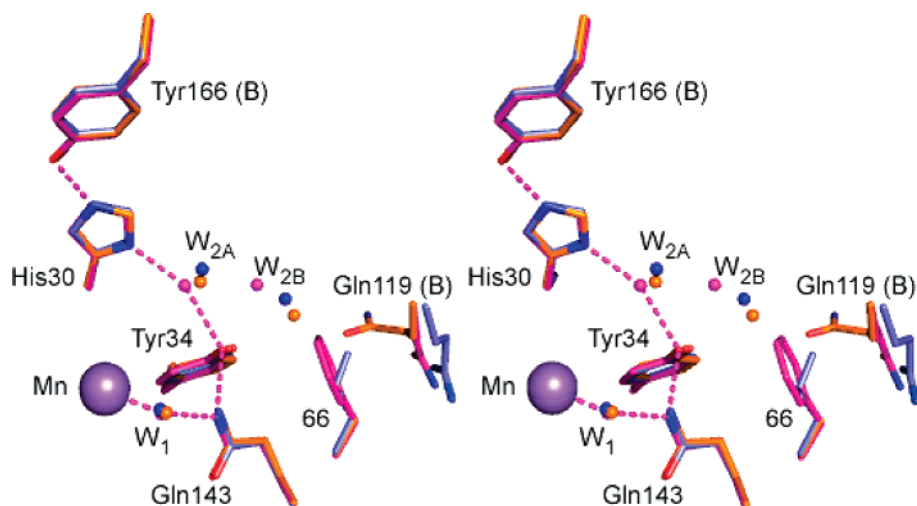
FIGURE 5: Stereoview of the superposition of residues 34, 66, and 119 and solvent molecules W_1, W_{2A}, and W_{2B} in human wild-type (magenta), F66A (orange), and F66L MnSOD (blue). This figure was made using PYMOL (www.pymol.org).
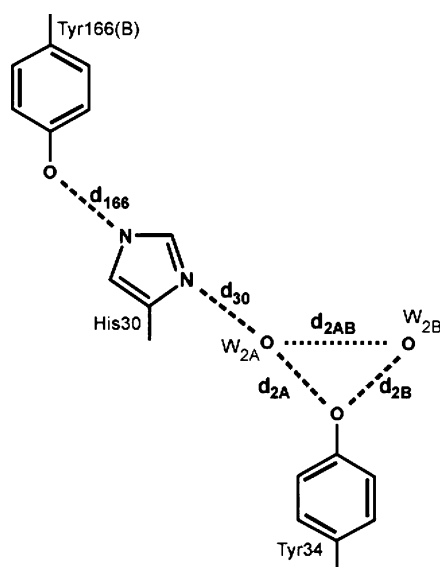

FIGURE 6: Schematic diagram depicting the distance geometry of selected solvent molecules and side chains in the active site and dimeric interface human MnSOD.

Table 3: Distance Geometry within the Active Site of Human Wild-Type, F66A, and F66L MnSOD and Wild-Type *E. coli* MnSOD As Shown in Figure 6[a]

	wild-type human	F66A	F66L	wild-type *E. coli*
d_{2A}	2.8	3.0	3.0	3.2
d_{2B}	2.9	2.7	3.3	2.6
d_{2AB}	2.9	4.0	3.8	2.7
d_{30}	2.6	2.9	2.9	2.8
d_{166}	2.7	2.6	2.6	2.6

[a] Distances are in angstroms.

human wild-type, F66A, and F66L MnSOD and *E. coli* MnSOD (Figure 7), whereas solvent molecule W_{2B} showed more disorder in *E. coli*, F66A, and F66L MnSOD than in human wild-type MnSOD. Interestingly, the normalized *B*-factor for W_{2A} was approximately the same for human wild-type and F66A MnSOD, whereas it was significantly less ordered in *E. coli* and human F66L MnSOD structures.

DISCUSSION

The conformations of the active sites of MnSOD from both eukaryotes and prokaryotes are generally superimposable,
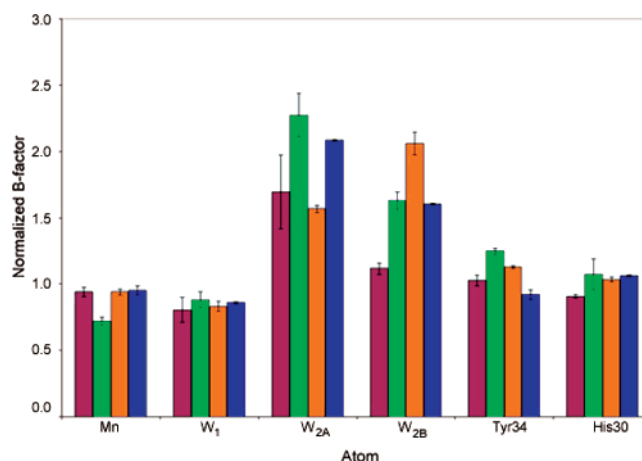

FIGURE 7: Histogram showing the normalized *B*-factors (Å^2) of the active-site manganese ion, solvent molecules W_1, W_{2A}, and W_{2B}, and side chains of Tyr34 and His30. Values are for wild-type human (magenta), wild-type *E. coli* (green), F66A (orange), and F66L (blue) MnSOD. Values are normalized to the average *B*-factor of the main chain atoms for the respective MnSOD. Error bars are normalized standard deviations.

as demonstrated in Figure 1 for human and *E. coli* MnSOD, yet the extent of product inhibition varies greatly. We replaced in human MnSOD a prominent residue Phe66 in a region of the dimeric interface showing significant structural differences between the human and *E. coli* enzymes (Figure 1). Phe66 in human MnSOD contributes to the environment of Tyr34 (Figure 1), a residue that affects product inhibition in human MnSOD (*14*, *17*) and has been thoroughly investigated in the *E. coli* enzyme (*15*, *16*, *18*).

We comment first that Phe66 is not essential for catalysis in human MnSOD. The large values of k_1 and k_2 for F66A and F66L MnSOD (Table 2), rate constants for catalysis (eqs 1 and 2), show that the variants we have studied were catalytically very active in comparison with wild-type human and *E. coli* MnSOD. However, there was a significant difference in the progress curves for catalysis as shown in Figure 2. Here it is apparent that F66A MnSOD demonstrates a region of zero-order catalysis consistent with many previous reports of product inhibition in MnSOD (*7*–*9*). In contrast, F66L MnSOD shows no apparent product inhibition under the conditions used for Figure 2. These conclusions are

expanded in the consideration of Figure 4. Here the absorbance of a short-lived intermediate at 420 nm appears for catalysis by human wild-type MnSOD, with a visible absorbance consistent with the product-inhibited complex (*7*, *11*). No such intermediate was observed for human F66L MnSOD and *E. coli* MnSOD under the conditions used for Figure 4.[2]

There are also notable differences when the kinetics of individual steps leading to product inhibition observed for the mutants are examined in comparison with those of human wild-type MnSOD. Product inhibition is assessed by two features of the catalysis. The first is the gating ratio k_2/k_3, the magnitude of which determines the rate of the uninhibited catalytic reduction of superoxide (eq 2) compared with the rate of formation of the inhibited complex (eq 3). The second is the rate constant k_4 for the dissociation of the inhibited complex (eq 4). The ratio k_2/k_3 determining the gating into the catalytic versus product-inhibited pathway is increased from 1 for the human wild type to 4 for F66L MnSOD (Table 2). This is a value near that of k_2/k_3 for *E. coli* MnSOD (Table 2) and reflects in significant part the cause of the weaker product inhibition observed for F66L MnSOD compared with wild-type human MnSOD.

The single-turnover results of Table 2 also show significant changes in k_4, the rate constant for the dissociation of the inhibited complex (eq 4). For each of the mutants of human MnSOD, there is a significant decrease in k_4, by $\sim 30-60\%$, compared with the wild-type value. Each of the mutations of Table 2 caused a decrease in k_4 to a value closer to that observed for *E. coli* MnSOD. The values of k_4 are a contributing factor but not the dominant factor in product inhibition. This is evident in an examination of the values of k_4 in Table 2; F66L has the smallest value of k_4, yet this enzyme is less product inhibited than wild-type and F66A MnSOD (Figure 2).

Previous work reported site-specific mutants of human MnSOD with greater product inhibition than the wild type (*11*, *14*). In each case, however, the change in product inhibition arose from a decrease in k_2 rather than significant changes in k_3. The variant human H30N MnSOD exhibited less product inhibition than the wild type which was due mostly to a large value of k_4 (480 s^{-1}); H30N MnSOD also exhibited a k_2/k_3 gating ratio close to unity as in wild-type MnSOD (*23*). In this report, we have observed that the replacement of Phe66 with Leu has mimicked the rates of *E. coli* MnSOD in that the extent of product inhibition is decreased predominantly by an increase in the k_2/k_3 gating ratio caused by a decrease in k_3.

Several features of the crystal structures offer intriguing possibilities for explaining the altered catalysis and inhibition in F66A and F66L MnSOD. First, the most striking structural difference induced by these two mutants appeared in F66A, where the $\beta - \gamma$ carbon torsion angle of Gln119 was rotated 90° compared to that of human wild-type MnSOD causing the side chain of Gln119 to point toward the active site and the manganese, thus occupying the void left by the replacement of Phe66 with Ala (Figure 5). This conformational change for F66A had smaller effects on k_3 and k_4 than the conformational changes of F66L (Table 2). However, there is evidence that another feature of the structures, the solvent in the active site, is significant in describing product inhibition.

The ordered water observed in the active site of MnSOD crystal structures appears to be relevant to the differences in product inhibition seen in our data. The distances between oxygen atoms in the network of ordered waters are mostly consistent with hydrogen bonding (Table 3 and Figure 6). However, two distances for F66A and F66L are too large to attribute to hydrogen bonds, specifically, d_{2AB}, the distance between W_{2A} and W_{2B}. In addition, the mobilities of ordered water molecules W_{2A} and W_{2B} observed in the crystal structures are large compared with that of W_1 and the side chains of Tyr34 and His30 (Figure 7) and overall are larger for the F66L, F66A, and *E. coli* forms than for human wild-type MnSOD. Also of possible significance is the normalized B-factor for W_{2A} that is approximately the same for human wild-type and F66A MnSOD, whereas it becomes significantly less ordered in the less product inhibited *E. coli* and human F66L MnSOD (Figure 7). These observations suggest a more dynamic and solvent accessible water cluster in the active site of the mutants and wild-type *E. coli* than in the human wild-type form. This may be in part why they are less product-inhibited as they may be able to enhance the k_2/k_3 gating ratio by promoting the formation of the product H_2O_2 more efficiently and slowing the formation of the peroxo complexes that lead to product inhibition. Work is in progress to extend these ideas to other site-specific mutants of human MnSOD.

Further evidence for the relevance of the solvent network is presented in consideration of solvent structures in relation to k_4. There is strong evidence from solvent H−D isotope effects that the dissociation of the product-inhibited complex described by k_4 contains a rate-contributing proton transfer (*11*). Decreased values of k_4 were observed for F66L and F66A MnSOD as well as *E. coli* MnSOD (Table 2). These are all variants associated with enhanced B-factors compared with those of human wild-type MnSOD. The increased mobility of waters W_{2A} and W_{2B} indicated by their normalized B-factors may imply that these residues have lost some of their ability to support proton transfer. The implication is that a less ordered water structure is related to less efficient proton transfer which accounts for the lower values of k_4. Another point to note is that the kinetic data for F66A MnSOD were complex and difficult to interpret. There was definitely an effect of pH on the values of k_4 for this variant, but it was not possible to quantify within the limitations of the kinetic measurements. The source of this may lie in fluxional behavior of the enzyme.

In summary, we have demonstrated that mutation of residue 66 provides a means of modulating to different extents the rates of the two alternate reactions open to superoxide and reduced MnSOD. Thus, we have succeeded in modulating the balance between production of H_2O_2 and formation of an inhibited complex, primarily by decreasing the rate of formation of the inhibited complex accompanied by smaller decreases in the rate constants associated with productive turnover. The replacement of Phe66 with Leu resulted in a mutant of human MnSOD with weakened product inhibition resembling that of *E. coli* MnSOD. Moreover, the mechanism of this weakened product inhibition was similar to that in *E. coli* MnSOD, specifically a decrease in the rate constant for the oxidative addition of superoxide to Mn^{2+}MnSOD leading to the reversible formation of the peroxide-inhibited enzyme. Crystallographic data

suggest that solvent structure and mobility as well as side chain conformations may affect the extent of product inhibition.

SUPPORTING INFORMATION AVAILABLE

A pH profile of k_4 catalyzed by human F66A MnSOD. This material is available free of charge via the Internet at http://pubs.acs.org.

REFERENCES

1. Fridovich, I. (1975) Superoxide dismutases, *Annu. Rev. Biochem. 44*, 147−159.
2. Fridovich, I. (1997) Superoxide anion radical, superoxide dismutases, and related matters, *J. Biol. Chem. 272*, 18515−18517.
3. Miller, A. F. (2004) Superoxide dismutase: Active sites that save, but a protein that kills, *Curr. Opin. Chem. Biol. 8*, 162−168.
4. Borgstahl, G. E., Parge, H. E., Hickey, M. J., Beyer, W. F., Jr., Hallewell, R. A., and Tainer, J. A. (1992) The structure of human mitochondrial manganese superoxide dismutase reveals a novel tetrameric interface of two 4-helix bundles, *Cell 71*, 107−118.
5. Lah, M. S., Dixon, M. M., Pattridge, K. A., Stallings, W. C., Fee, J. A., and Ludwig, M. L. (1995) Structure-function in *Escherichia coli* iron superoxide dismutase: Comparisons with the manganese enzyme from *Thermus thermophilus*, *Biochemistry 34*, 1646−1660.
6. Smith, M. W., and Doolittle, R. F. (1992) A Comparison of Evolutionary Rates of the 2 Major Kinds of Superoxide Dismutase, *J. Mol. Evol. 34*, 175−184.
7. Bull, C., Niederhoffer, E. C., Yoshida, T., and Fee, J. A. (1991) Kinetic-Studies of Superoxide Dismutases: Properties of the Manganese-Containing Protein from *Thermus thermophilus*, *J. Am. Chem. Soc. 113*, 4069−4076.
8. McAdam, M. E., Fox, R. A., Lavelle, F., and Fielden, E. M. (1977) A pulse-radiolysis study of the manganese-containing superoxide dismutase from *Bacillus stearothermophilus*. A kinetic model for the enzyme action, *Biochem. J. 165*, 71−79.
9. Hsu, J. L., Hsieh, Y., Tu, C., O'Connor, D., Nick, H. S., and Silverman, D. N. (1996) Catalytic properties of human manganese superoxide dismutase, *J. Biol. Chem. 271*, 17687−17691.
10. Abreu, I. A., Hearn, A., An, H., Nick, H. S., Silverman, D. N., and Cabelli, D. E. (2007) The kinetic mechanism of manganese-containing superoxide dismutase from *Deinococcus radiodurans*: A specialized enzyme for the elimination of high superoxide concentrations (submitted).
11. Hearn, A. S., Stroupe, M. E., Cabelli, D. E., Lepock, J. R., Tainer, J. A., Nick, H. S., and Silverman, D. N. (2001) Kinetic analysis of product inhibition in human manganese superoxide dismutase, *Biochemistry 40*, 12051−12058.
12. Davis, C. A., Hearn, A. S., Fletcher, B., Bickford, J., Garcia, J. E., Leveque, V., Melendez, J. A., Silverman, D. N., Zucali, J., Agarwal, A., and Nick, H. S. (2004) Potent anti-tumor effects of an active site mutant of human manganese-superoxide dismutase. Evolutionary conservation of product inhibition, *J. Biol. Chem. 279*, 12769−12776.
13. Ramilo, C. A., Leveque, V., Guan, Y., Lepock, J. R., Tainer, J. A., Nick, H. S., and Silverman, D. N. (1999) Interrupting the hydrogen bond network at the active site of human manganese superoxide dismutase, *J. Biol. Chem. 274*, 27711−27716.
14. Greenleaf, W. B., Perry, J. J., Hearn, A. S., Cabelli, D. E., Lepock, J. R., Stroupe, M. E., Tainer, J. A., Nick, H. S., and Silverman, D. N. (2004) Role of hydrogen bonding in the active site of human manganese superoxide dismutase, *Biochemistry 43*, 7038−7045.
15. Maliekal, J., Karapetian, A., Vance, C., Yikilmaz, E., Wu, Q., Jackson, T., Brunold, T. C., Spiro, T. G., and Miller, A. F. (2002) Comparison and contrasts between the active site pKs of Mn-superoxide dismutase and those of Fe-superoxide dismutase, *J. Am. Chem. Soc. 124*, 15064−15075.
16. Whittaker, M. M., and Whittaker, J. W. (1997) Mutagenesis of a proton linkage pathway in *Escherichia coli* manganese superoxide dismutase, *Biochemistry 36*, 8923−8931.
17. Guan, Y., Hickey, M. J., Borgstahl, G. E., Hallewell, R. A., Lepock, J. R., O'Connor, D., Hsieh, Y., Nick, H. S., Silverman, D. N., and Tainer, J. A. (1998) Crystal structure of Y34F mutant human mitochondrial manganese superoxide dismutase and the functional role of tyrosine 34, *Biochemistry 37*, 4722−4730.
18. Edwards, R. A., Whittaker, M. M., Whittaker, J. W., Baker, E. N., and Jameson, G. B. (2001) Outer sphere mutations perturb metal reactivity in manganese superoxide dismutase, *Biochemistry 40*, 15−27.
19. Carlioz, A., and Touati, D. (1986) Isolation of superoxide dismutase mutants in *Escherichia coli*: Is superoxide dismutase necessary for aerobic life? *EMBO J. 5*, 623−630.
20. Edwards, R. A., Baker, H. M., Whittaker, M. M., Whittaker, J. W., Jameson, G. B., and Baker, E. N. (1998) Crystal structure of *Escherichia coli* manganese superoxide dismutase at 2.1 Angstrom resolution, *J. Biol. Inorg. Chem. 3*, 161−171.
21. Cabelli, D. E., Guan, Y., Leveque, V., Hearn, A. S., Tainer, J. A., Nick, H. S., and Silverman, D. N. (1999) Role of tryptophan 161 in catalysis by human manganese superoxide dismutase, *Biochemistry 38*, 11686−11692.
22. Otwinowski, Z., and Minor, W. (1997) Processing of X-ray Diffraction Data Collected in Oscillation Mode, *Methods Enzymol. 276*, 307−326.
23. Hearn, A. S., Stroupe, M. E., Cabelli, D. E., Ramilo, C. A., Luba, J. P., Tainer, J. A., Nick, H. S., and Silverman, D. N. (2003) Catalytic and structural effects of amino acid substitution at histidine 30 in human manganese superoxide dismutase: Insertion of valine Cγ into the substrate access channel, *Biochemistry 42*, 2781−2789.
24. Collaborative Computational Project, Number 4 (1994) The CCP4 Suite: Programs for Protein Crystallography, *Acta Crystallogr. D50*, 760−763.
25. Vagin, A., and Teplyakov, A. (1997) MOLREP: An automated program for molecular replacement, *J. Appl. Crystallogr. 30*, 1022−1025.
26. Brunger, A. T., Adams, P. D., Clore, G. M., DeLano, W. L., Gros, P., Grosse-Kunstleve, R. W., Jiang, J. S., Kuszewski, J., Nilges, M., Pannu, N. S., Read, R. J., Rice, L. M., Simonson, T., and Warren, G. L. (1998) Crystallography & NMR system: A new software suite for macromolecular structure determination, *Acta Crystallogr. D54*, 905−921.
27. Emsley, P., and Cowtan, K. (2004) Coot: Model-building tools for molecular graphics, *Acta Crystallogr. D60*, 2126−2132.
28. Rabani, J., and Nielsen, S. O. (1969) Absorption spectrum and decay kinetics of superoxide in aqueous solutions by pulse radiolysis, *J. Phys. Chem. 73*, 3736.
29. Miller, A.-F., Padmakumar, D., Sorkin, D. L., Karapetian, A., and Vance, C. (2003) Proton-coupled electron transfer in FeSOD and MnSOD, *J. Inorg. Biochem. 93*, 71−83.
30. Leveque, V. J., Vance, C. K., Nick, H. S., and Silverman, D. N. (2001) Redox properties of human manganese superoxide dismutase and active-site mutants, *Biochemistry 40*, 10586−10591.
31. Abad, M. F. C., Di Benedetto, G., Magalhaes, P. J., Filippin, L., and Pozzan, T. (2004) Mitochondrial pH monitored by a new engineered green fluorescent protein mutant, *J. Biol. Chem. 279*, 11521−11529.
32. Borgstahl, G. E. O., Pokross, M., Chehab, R., Sekher, A., and Snell, E. H. (2000) Cryo-trapping the six-coordinate, distorted-octahedral active site of manganese superoxide dismutase, *J. Mol. Biol. 296*, 951−959.